Electrochimica Acta 76 (2012) 446–452

Contents lists available at SciVerse ScienceDirect

Electrochimica Acta

journal homepage: www.elsevier.com/locate/electacta

Effect of Au nano-particles on TiO_2 nanorod electrode in dye-sensitized solar cells

M. Ghaffari[a,b,*], M. Burak Cosar[c,d], Halil I. Yavuz[c,d], M. Ozenbas[c,d], Ali K. Okyay[a,b,*]

[a] UNAM – Institute of Materials Science and Nanotechnology, Bilkent University, Ankara 06800, Turkey
[b] Department of Electrical and Electronics Engineering, Bilkent University, Ankara 06800, Turkey
[c] Department of Metallurgical and Materials Engineering, Middle East Technical University, Ankara 06800, Turkey
[d] Center for Solar Energy Research and Applications (GUNAM), Middle East Technical University, Ankara 06800, Turkey

ARTICLE INFO

Article history:
Received 9 March 2012
Received in revised form 4 May 2012
Accepted 17 May 2012
Available online 26 May 2012

Keywords:
Dye-sensitized solar cell
Hydrothermal
TiO_2 nanorods
Photoreduction

ABSTRACT

Au nano particles (NPs) were deposited on vertically grown TiO_2 nanorod arrays on FTO substrate by hydrothermal process. Metal nanoparticles were loaded onto the surface of TiO_2 nanorods via photochemical reduction process under ultraviolet irradiation. X-ray diffraction (XRD), electron microscopy (FESEM), transmission electron microscopy (TEM) and X-ray photoelectron spectroscopy (XPS) analysis were used to characterize the as-prepared Au/TiO_2 nanorod composites. Current density–voltage (J–V) measurements were obtained from a two-electrode sandwich type cell. The presence of Au nanoparticles can help the electron–hole separation by attracting photoelectrons. Addition of Au nanoparticles to the TiO_2 nanorod significantly increased the fill factor and J_{SC} (short circuit current density). The application of Au NPs TiO_2 nanorods in improving the performance of DSSCs is promising.

1. Introduction

Since the first report by Gratzel et al. in 1991, dye sensitized solar cells (DSSC) have attracted extraordinary attention. DSSCs could be viable low cost alternatives to silicon-based solar cells [1,2]. Initial demonstrations of DSSCs were based on dye sensitization of porous nano crystalline semiconductors like TiO_2. There are numerous studies on the potentials of improving the efficiency of DSSCs by using other semiconducting metal oxides, such as Nb_2O_5 [3], CeO_2 [4], ZnO [5,6], and SnO_2 [7] and composite oxide materials [8,9].

Synthesis of aligned single-crystalline TiO_2 nanorods or nanowires has attracted extensive attention because of their excellent and unique potential applications in electronics, photochemistry, biology and optics, as well as their applications in gas sensors [10], dye-sensitized solar cells [11], lithium ion batteries [12], photovoltaic devices [2], and as photocatalysts [13].

Recently, numerous methods for fabricating one-dimensional nanostructured TiO_2 have been reported, such as template-assisted synthesis [14], sol–gel [15], chemical vapor deposition [16], electrochemical etching [17], and hydrothermal [18–20]. Among these techniques, the hydrothermal method of TiO_2 nanorod arrays is a promising technique owing to its scalability, simple process, and low cost. The potential advantages of the hydrothermal growth method may be partially hindered by the growth of rutile phase TiO_2 nanorods. In order to achieve high efficiency DSSCs, TiO_2 in anatese form is desirable, which may be obtained by a post-growth-coating method such as atomic layer deposition technique.

DSSC efficiencies could be improved significantly by using single crystal nanorods of TiO_2 instead of nanoparticles which could promote the efficient transport of photogenerated electrons [21–23]. The crystal structure of TiO_2 also plays a factor in efficiency of DSSCs [24–27]. The difference between the conduction band levels of anatase and rutile forms, however due to the low difference between the conduction band levels of anatase and rutile, the higher diffusion coefficient of anatase play more important role for the efficient electron transport in anatase [28] and therefore, favors the use of pure anatase for DSSC applications [24]. There are reports, however, that synergistic use of rutile and anatase polymorphs of TiO_2 nanoparticles could increase DSSC efficiency [24,25,27]. Such an effect is also observed in photocatalytic activity of anatase TiO_2 nano crystals, which significantly increases upon mixing with a portion of lesser active rutile nano crystals [29,30]. On the contrary, there are some reports claiming better efficiency DSSCs with pure anatase form [31], however, a conclusive comparison cannot be obtained because size and morphology of the particles were also varied in those studies.

In DSSCs, at the semiconductor/electrolyte interface, the recombination of a portion of the electrons is still inevitable. There are several studies to decrease this undesired reaction at the interface of semiconductor/electrolyte by using core-shell structure of various metal oxides [6,32,33] or by using different additives in the

* Corresponding authors at: UNAM – Institute of Materials Science and Nanotechnology, Bilkent University, Ankara 06800, Turkey. Tel.: +90 544 3839 429.
E-mail addresses: ghaffari@unam.bilkent.edu.tr, moha0094@e.ntu.edu.sg (M. Ghaffari), aokyay@ee.bilkent.edu.tr (A.K. Okyay).

0013-4686/$ – see front matter © 2012 Elsevier Ltd. All rights reserved.
http://dx.doi.org/10.1016/j.electacta.2012.05.058

electrolyte to passive the electrolyte-exposed [34–37]. Moreover there are a number of earlier reports showing that addition of metal nanoparticles improves DSSC energy conversion efficiency [38–41].

In this study, Au NPs act to prevent charge carrier recombination by forming a Schottky energy barrier that promotes the photo-injected electrons into the nanorod, away from the surface which improves the overall conversion efficiency of the DSSCs with Au NPs/TiO_2 nanorod structure. Shii Chou et al. [41] have reported dye sensitized solar cell based on the TiO_2/nano-metal composite particles using the dry coating process in a mechano-fusion system, and studied the effect of nano-metallic particles on the performance of the cell and obtained a lower efficiency of 0.29%. In our research, Au NPs were deposited on TiO_2 nanorod arrays by photoreduction before dye absorption, and an overall conversion efficiency of 0.93% was obtained for Au NPs/TiO_2 structure which is a threefold higher relative to devices without Au NPs.

There are several parameters that can affect the efficiency of DSSCs based on hydrothermal-grown TiO_2 nanorod arrays such as growth time, growth temperature, substrates, initial reactant concentration, acidity, titanium precursors and $TiCl_4$ treatment. By optimizing these parameters, it is possible to obtain high efficiency DSSCs [22,42]. In this study, we comparatively study the effect of Au NPs on DSSC efficiency by defining a baseline (with no Au NPs) device as reference.

2. Experimental procedure

2.1. Chemical

FTO glass substrate (F: SnO_2, Tec 15 Ω/sq.) with a thickness of 4 mm was purchased from Pilkington, England. Ethanol, acetone, titanium butoxide ($Ti(OCH_2CH_2CH_2CH_3)_4$) (97%), $HAuCl_4$ (Mw = 339.79), and HCl (36%) were from Sigma–Aldrich Co. All chemicals were of analytical grade and were used as received. Hydrothermal growth was carried out in a 45 ml teflon-lined autoclave. Deionized water was used to prepare all the solutions.

2.2. Growth of TiO_2 nanorod array

The dimension of FTO glass substrate was 10 mm × 50 mm and was cleaned and degreased prior to use, first by washing with detergent and distilled water, then were ultrasonically cleaned with ethanol and then by sonicating in ethanol, acetone and deionized water in sequence for about 30 min, and finally dried under nitrogen flow. 20 mL concentrated hydrochloric acid (36% by weight) was mixed with 20 mL deionized water in a teflon-lined stainless steel autoclave (45 mL vol.). The mixture was stirred at ambient conditions for 10 min, and then 0.8 mL titanium butoxide was added into the above mentioned solution and stirred for 30 min. Conducting side of FTO substrate was faced down with an angle against the wall of the teflon vessel. Sample was kept at 140 °C for 4 h in an electrical oven. The sample and teflon vessel was unloaded and let to cool to room temperature. The FTO substrate rinsed with deionized water and ethanol, and then dried in air.

2.3. Deposition of Au nanoparticles on TiO_2 nanorods by photoreduction

20 μL (2.5 mmol/L) $HAuCl_4$ of aqueous Au salt solution were dispersed with 15 mL of deionized water in a pyrex petri dish with capacity of about 20 mL. Then the TiO_2 nanorods grown on FTO substrate were floated in the petri dish and exposed under UV light (254 nm) from a UVP company, EL series (8 W, UVLMS-38 EL, 376 mm × 96 mm × 64 mm). The reactions were carried for 3 and 9 h. Then the sample was washed by deionized water and ethanol. Finally, the samples were dried at room temperature.

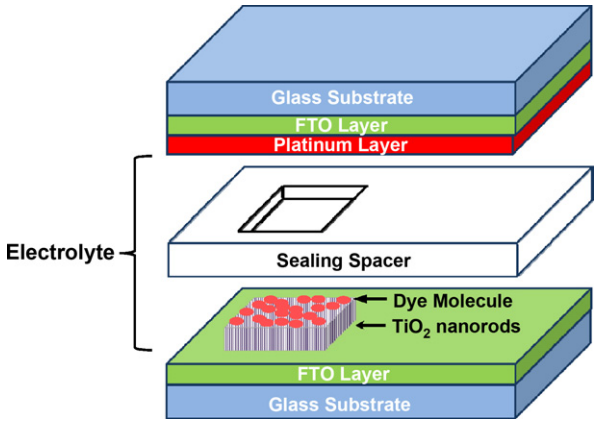

Fig. 1. Schematic sketch of assembled dye sensitized solar cell.

2.4. Materials characterization

The phase structures of the obtained samples were identified using a Pananalytical (X'pert Pro MPD) instrument. XRD patterns were collected over the 2θ angular range of 10–80° using Bragg–Brentano geometry (Cu Kα source, primary and secondary Soller slits, 0.1 mm divergence slits, 0.3 mm receiving slit, and secondary graphite monochromator). The morphology and structural characteristics of the obtained samples were studied by scanning electron microscopy (FESEM, FEI–Nova Nanosem 430), and transmission electron microscopy (TEM, FEI–Tecnai G2F30). The surface chemical composition of the Au/TiO_2 nanorods was monitored by X-ray photoelectron spectroscopy (XPS) measurements, performed with a Thermo (K-Alpha – Monochromated High-performance XPS Spectrometer) instrument.

2.5. Electrode fabrication and characterization techniques

A schematic diagram of assembled dye sensitized solar cell is presented in Fig. 1. The active area of electrode was 0.25 cm^2 (i.e. 5 mm × 5 mm). Synthesized TiO_2 electrodes were soaked in 0.5 mmol/l ruthenium sensitizer dye [cis-di(thiocyanato)-*N*-*N*′-bis(2,2′-bipyridyl-4-carboxylic acid-4′-tetrabutylammonium carboxylate) ruthenium (II)] dye (known as N719, Solaronix) in a *t*-butanol/acetonitrile (1:1, in volume ratio) solution, for 24 h. The sensitized electrodes were rinsed with acetonitrile, dried in room temperature, and immediately used for measuring photovoltaic properties. The platinum coated FTO glass was used as counter electrodes bonded to TiO_2 nanorods as working electrode by 25-μm-thick hot-melt spacers made of the ionomer Surlyn 1702 (Dupont). The internal space of each cell was filled with a liquid electrolyte. The electrolyte was composed of 0.1 M guanidinium thiocyanate (GuSCN), 0.03 M I2, 0.5 M 4-*tert*-butylpyridine (TBP) and 0.6 M butylmethylimidazolium iodide (BMII) in the mixture of acetonitrile and valeronitrile (85:15, in vol.%). The devices were characterized by a Keithley 2440 source meter under standard AM1.5 G-filtered irradiation (100 mW/cm^2) from a Newport 91192 solar simulator equipped with 300 W xenon arc. The spectral measurements are obtained by a mechanically chopped monochromated (Newport Cornerstone 130 1/8 m, 1200 L/mm) white-light source and a lock-in amplifier (SRS 830). The spectral intensity of the light source is also separately characterized and is used to normalize the measured current.

3. Results and discussion

To identify the crystalline structure and orientation of the nanorods grown, XRD analysis was performed on the obtained samples. The XRD pattern of the as-prepared TiO_2 nanorod array and the standard diffraction pattern of rutile structure of TiO_2 (JCPDS, 82-0514) is presented in Fig. 2. All diffraction peaks can be indexed to the FTO substrate and rutile phase of TiO_2 (tetragonal, P42/MNM). In comparison with the ICSD standard XRD pattern, XRD pattern of the aligned rutile TiO_2 grown on FTO shows the preferable orientation of the nanostructures along TiO_2 [1 0 1] ($2\theta \sim 26.4^\circ$).

The FESEM micrographs (Fig. 3(a) and (b)) presents highly ordered TiO_2 nanorods grown on the FTO substrates. These results confirm that well-aligned TiO_2 nanorods uniformly grew in large area. Cross-sectional FESEM image of TiO_2 nanorod array shown in Fig. 3(b) indicates that length of nanorods are about 2.1 μm. The nanorod diameter distribution was obtained from the FESEM images, which ranges from about 135 to 150 nm (Fig. 3(a)). Fig. 3(c) and (d) presents the TiO_2 nanorod samples with different amount of gold deposition that clearly shows the effect deposition time, 3 h and 9 h, respectively. Inset Fig. 3(c) and (d) shows that the Au NPs preferentially deposit on the tips of rods and top active part of nanorods are covered by Au NPs.

Fig. 4(a) shows the TEM image of a single TiO_2 nanorod and corresponding selected area electron diffraction pattern (SAED). The TEM micrograph shows that the diameter of TiO_2 nanorod is 148 nm. The SAED and HRTEM results further confirm that each individual TiO_2 nanorod is single crystal. The lattice fringe spacing in the HRTEM image is 0.32 nm which corresponds to the interspacing of the (1 1 0) planes of tetragonal rutile structure of TiO_2 and indicates that the growth occurred along the [1 0 1] direction.

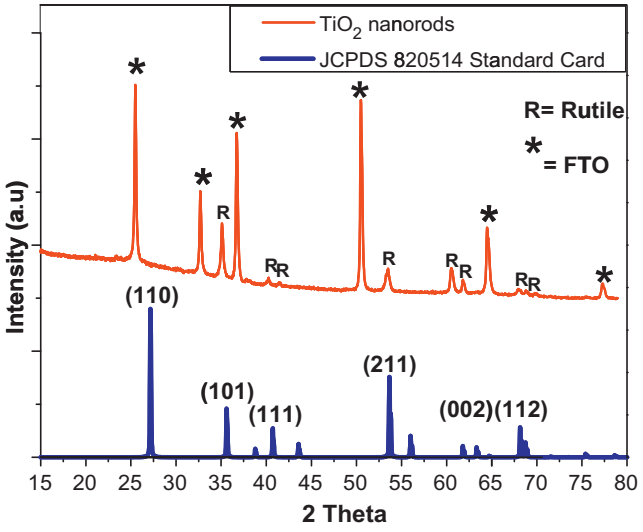

Fig. 2. XRD pattern of TiO_2 nanorod arrays on FTO substrate (*), and the standard diffraction pattern of rutile structure of TiO_2 (JCPDS-82-0514 standard card).

TEM micrographs of the Au NPs deposited on TiO_2 nanorods are shown in Fig. 5(a) and (b) which confirm that Au NPs deposited

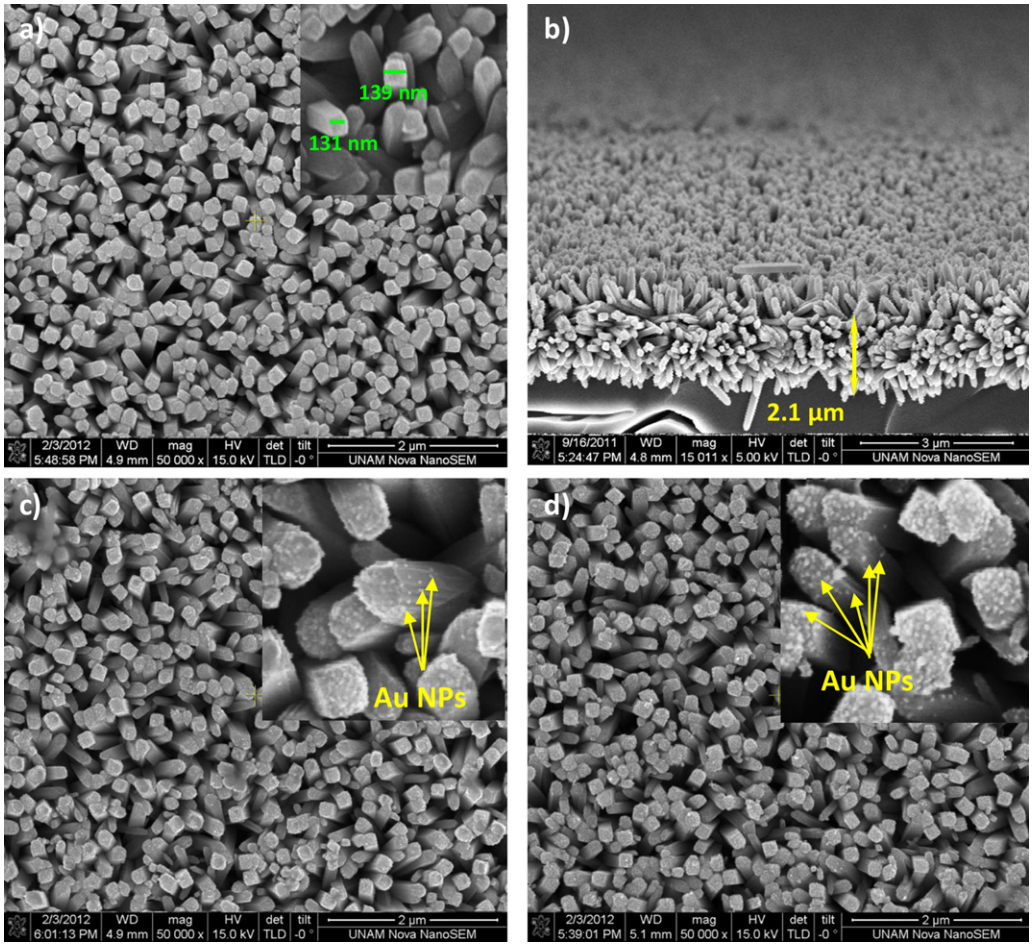

Fig. 3. SEM micrographs of well-aligned TiO_2 nanorod arrays: (a) top view and (b) side view (c) with 1.54 at % Au (d) with 3.4 at % Au.

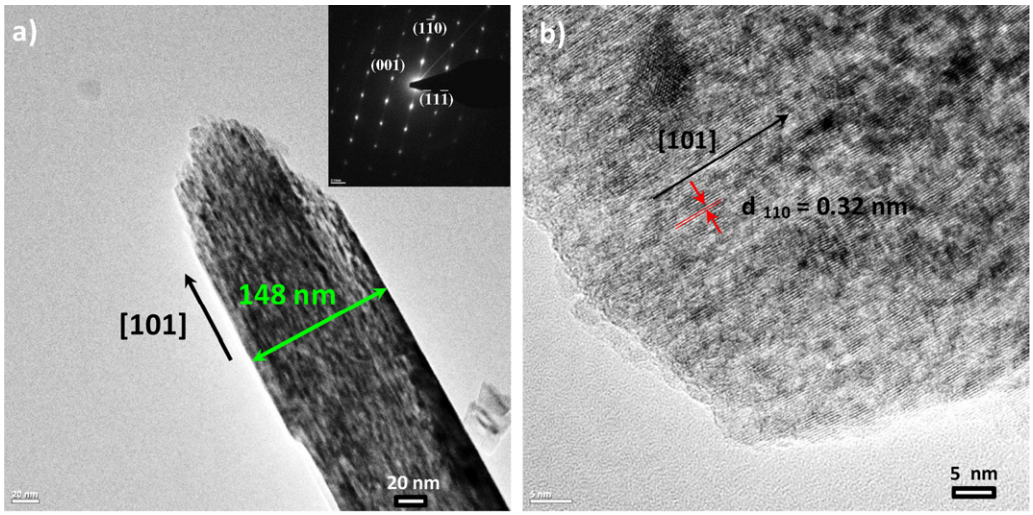

Fig. 4. TEM micrographs of rutile TiO_2 (1 1 0) (a) low-magnification image, and corresponding selected area electron diffraction pattern (SAED) and (b) high-resolution TEM micrograph.

on the surface of TiO_2 nanorods. This is attributed to a top illumination and low penetration of UV light into the rods along their growth axis hence most of the reduction reaction occurring on the tip area of nanorods. Fig. 5(b) also shows that the size of Au NPs is about 8–12 nm. Fig. 5(d) shows the corresponding SAED of Au NPs deposited on TiO_2 nanorods. The ring diffraction pattern clearly confirmed that structure of deposited Au nano particles are polycrystalline.

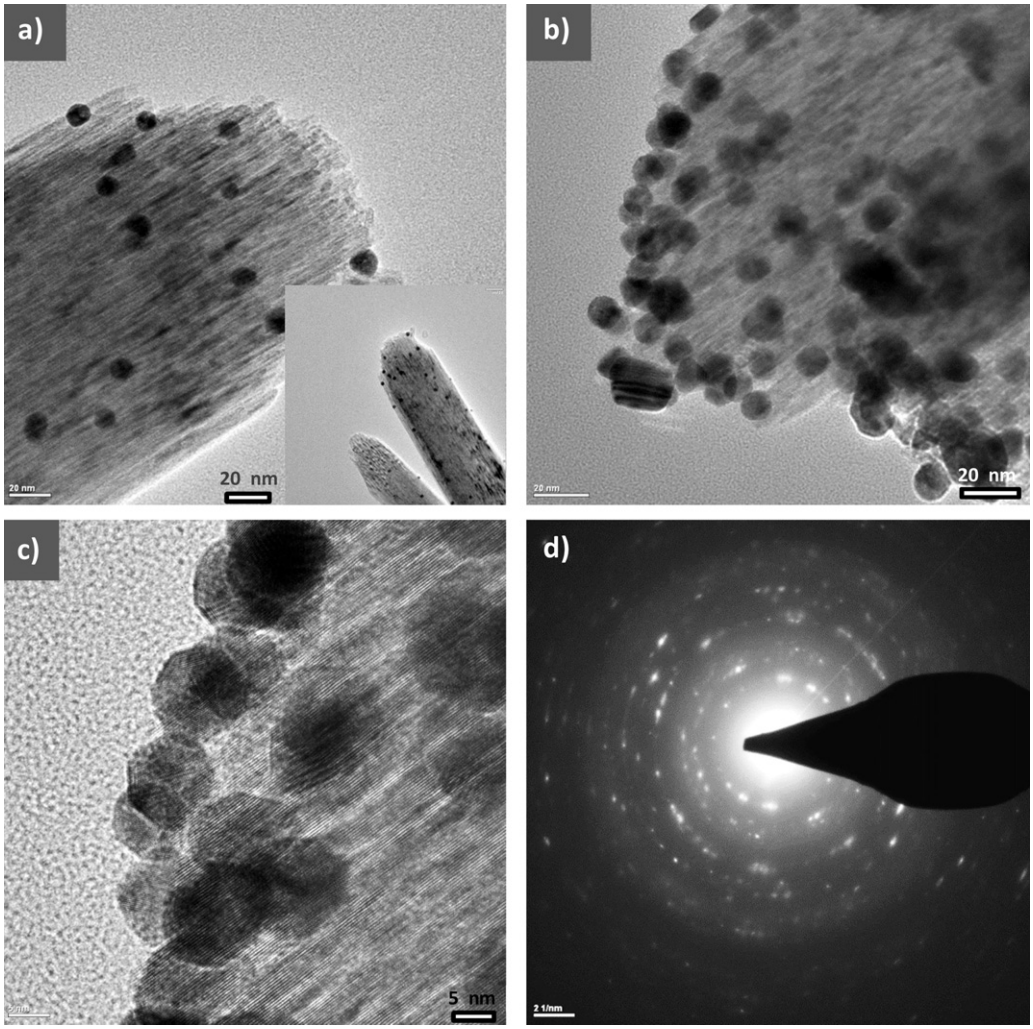

Fig. 5. TEM micrographs of Au NPs deposited on TiO_2 nanorods (a) low-magnification image of 1.54 at.% Au deposition, (b) low-magnification image of 3.4 at.% Au deposition, (c) high-magnification image of 3.4 at.% Au deposition, and (d) corresponding selected area electron diffraction pattern (SAED).

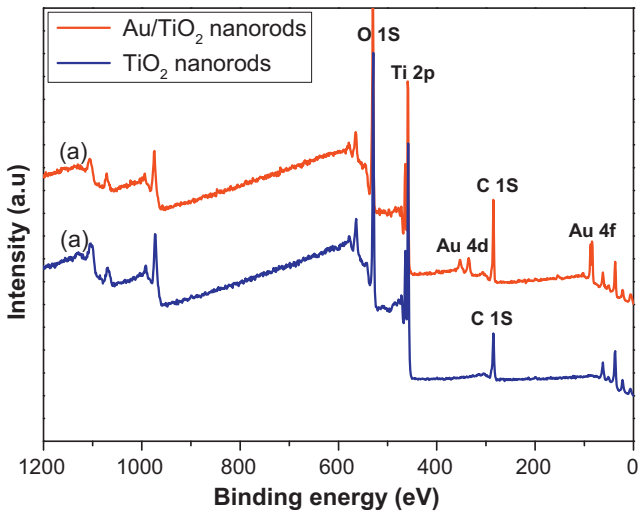

Fig. 6. Wide scan survey XPS spectrum of (a) TiO_2 nanorod arrays, and (b) Au/TiO_2 nanorod arrays.

The surface composition of the obtained samples was characterized by X-ray photoelectron spectroscopy (XPS) technique. XPS survey-scan spectrum of TiO_2 nanorods and Au-NP decorated TiO_2 nanorods are shown in Fig. 5(a). All XPS spectral peaks were fitted with Thermo Scientific Avantage software. As required by theory, the Ti 2p and Au 4f spectrum consist of two peaks, a spin–orbit doublet whereas O 1s and C 1s spectral lines consist of a single peak (a singlet). The C 1s spectral line was standardized to 285.0 eV and the O 1s, Ti 2p and Au 4f spectra were adjusted to this energy. The data analysis involved curve-fitting Lorentzian–Gaussian (30% Lorentzian) line shapes, spectra normalization, and Shirley background subtraction [43]. In all fits to narrow scan spectra Shirley backgrounds were used [44,45].

Fig. 6 presents the survey scan of prepared samples. The XPS peaks with binding energies of 84.03, 458.501 and 529.96 eV correspond to Au 4f, Ti 2p3/2 and O 1s, respectively. The Au 4f spectra serve as evidence for the formation of Au NPs on the TiO_2 nanorods.

Fig. 7 shows O 1s XPS spectra for the Au/TiO_2 nanorods (Fig. 7(a)) and TiO_2 nanorods (Fig. 7(b)) samples. Deconvolution of the O 1s

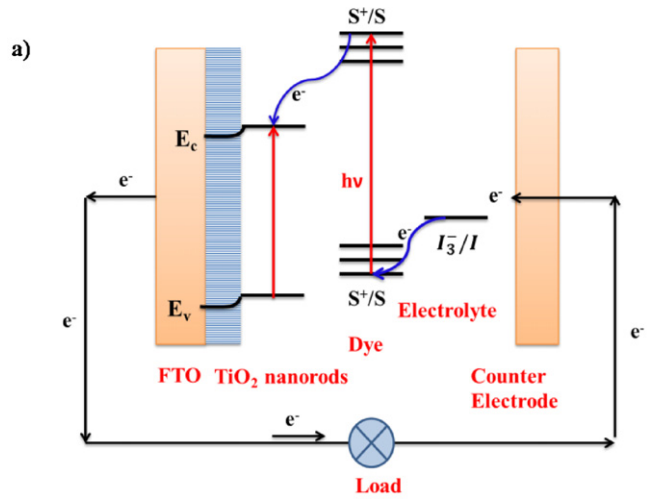

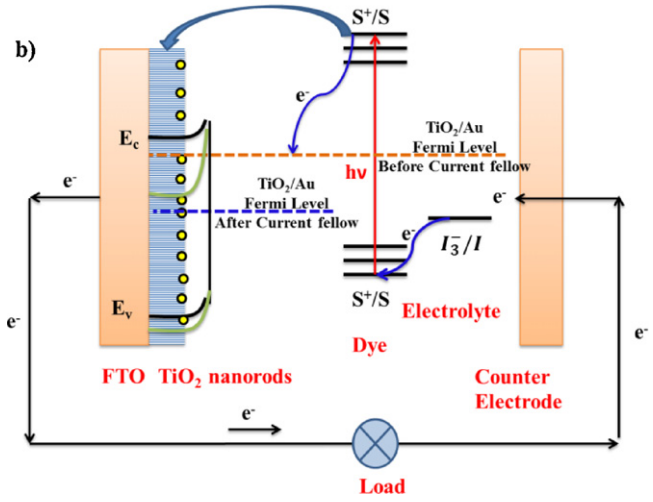

Fig. 8. Schematic diagram of the principle of (a) the conventional DSSC, and (b) the DSSC with Au NPs deposited on TiO_2 nanorods DSSC. (For interpretation of the references to color in the text, the reader is referred to the web version of this article.)

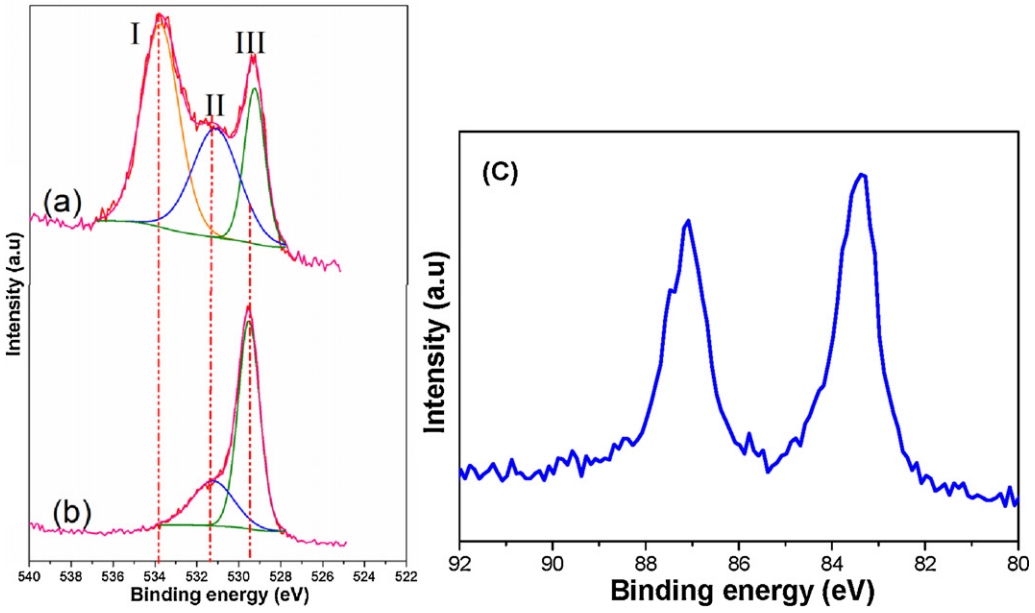

Fig. 7. XPS spectrum in the O 1s region for (a) TiO_2 nanorod and (b) Au/TiO_2 nanorod, and (c) narow scan of Au 4f.

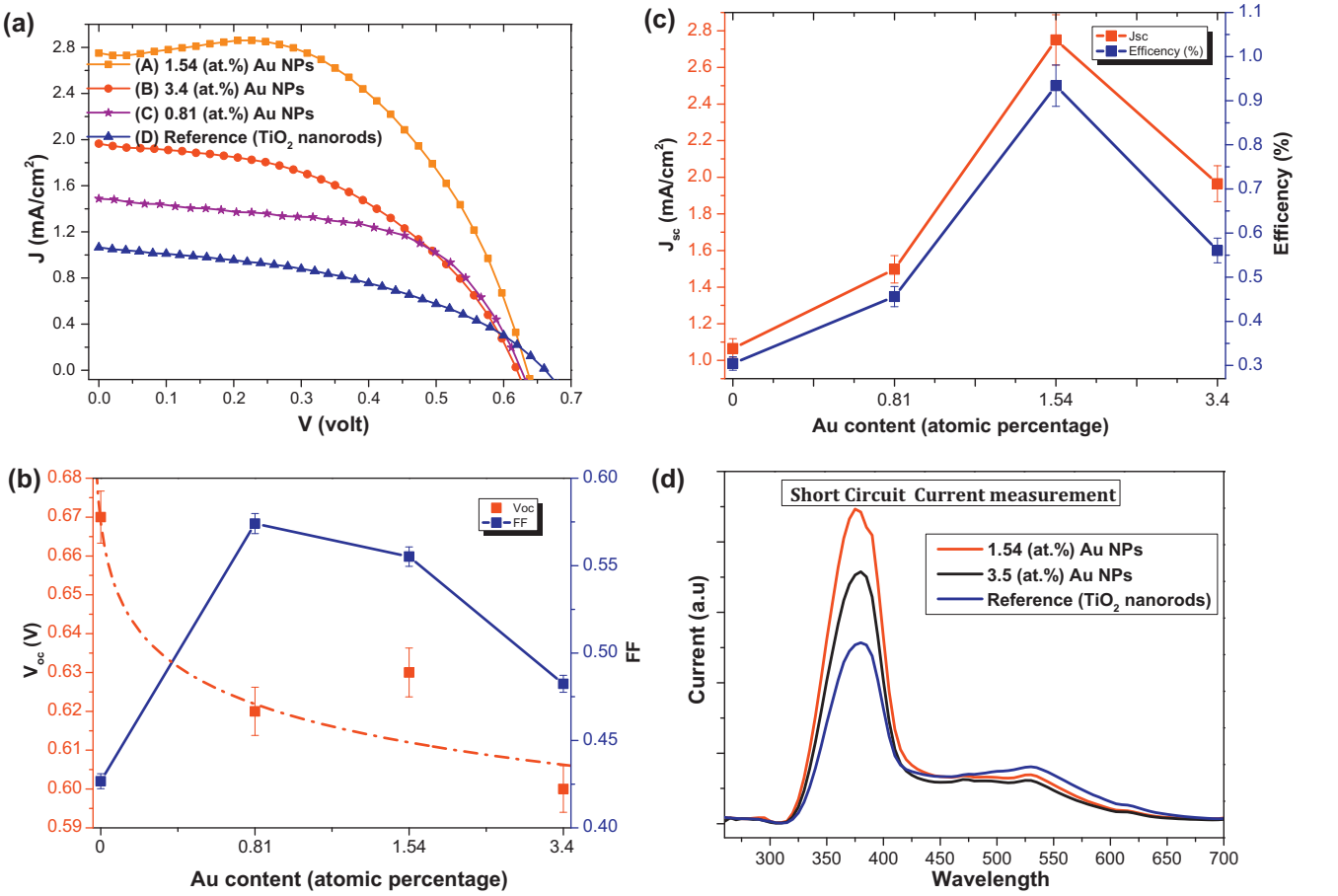

Fig. 9. (a) Current–voltage characteristics of the DSSCs assembled using the TiO_2 nanorod arrays, and the Au/TiO_2 nanorod with different gold content; (b) dependence of fill factor and V_{OC} on the amount of Au NPs content deposition; (c) dependence of cell efficiency and J_{SC} on the amount of Au NPs content deposition of the TiO_2 nanorod cells; and (d) short circuit current measurement vs. wavelength.

spectra yields three individual peaks at 529.7, 531.58 and 532.64 eV. Regarding the literature the oxygen peak located at 529.7 eV is related to the O 1s band position of TiO_2 [46,47]. Fig. 7(c) shows the detailed peak scan of Au 4f which confirms the presence of peaks with a binding energy of 83.35 eV and 87.14 eV corresponding to Au 4f 5/2 and Au 4f 3/2, respectively [9,45]. Sham and Lazarus explained that ambient TiO_2 samples are always covered with physisorbed moisture and chemisorbed and the O 1s binding energies for this surface shifts to higher binding energy. Thus O 1s peak at 531.5 eV can be assigned to oxygen species in H_2O molecules and Ti—OH while the peak at 533.7 eV is attributed to the water, hydroxide absorbed on the surface and (C—O—C or C—OH groups) from the oxidized carbon species of adventitious carbon [9,45]. The XPS results reveal that with deposition of Au NPs the amount of moisture and carbon species on surface of samples decreased dramatically.

In the Au/TiO_2 nanorod system, due to the larger work function of Au (5.1 eV) compared to the electron affinity of TiO_2 (3.2 eV), a Schottky barrier exists at their interface. Fig. 8 shows the schematic diagram of the possible electron-transfer path in the Au NPs TiO_2 nanorods DSSC and formation of the Schottky barrier between the Au NPs and TiO_2 nanorods. By (after) growing the Au NPs on the surface of TiO_2 nanorods, Fermi-level of the Au/TiO_2 nanorods attains a stable balance in equilibrium condition (orange dashed line in Fig. 8(b). Generated electron and hole pairs as a result of photo excitation process, create electric current which bend down the conduction and valence bands of Au/TiO_2 nanorods (the green curve in Fig. 8(b). Consequently the Au/TiO_2 nanorods Fermi level is pushed downward (the blue dashed line in Fig. 8(b). Moreover some of excited electrons can also be directly injected from the dye into the CB of the TiO_2 nanorods. Therefore, due to the existence of the Schottky barrier at the Au NPs and TiO_2 nanorods interface, electrons at the CB of TiO_2 nanorods cannot reverse their path, and flow towards the oxidized dye molecules or the redox electrolyte, thus leading to an improvement in the photocurrent [36,41].

Fig. 9(a) compares the TiO_2 nanorod solar cell and Au/TiO_2 nanorod solar cells. It compares *J–V* data from samples of Au NPs deposited with different gold concentration. In the plots a TiO_2 nanorod cell is included as reference. Deposition of Au NPs to TiO_2 nanorod cells caused significant improvement in efficiency, fill factor, and J_{SC} (Table 1). Fig. 9(b) presents that with increasing the Au NPs, the open-circuit voltage, V_{OC}, of obtained samples does not change significantly, which confirms that prepared cells are quite stable and no corrosive reaction occurs between Au NPs and the electrolyte [41]. On the contrary, short-circuit current J_{SC} of the Au NPs TiO_2 nanorods exceeds that of DSSC with no Au NPs (Fig. 9(c)).

Table 1
Efficiency (η), fill factor (FF), open circuit voltage (V_{OC}) and short circuit current density (J_{SC}) of dye-sensitized solar cells based on Au NPs deposited TiO_2 structure, and bare TiO_2 nanorod arrays.

Sample	Au NPs content (atomic percentage)	J_{SC} (mA/cm^2)	V_{OC} (V)	FF	η (%)
(A)	1.54	2.75	0.63	0.56	0.94
(B)	3.4	1.97	0.61	0.48	0.56
(C)	0.81	1.50	0.62	0.57	0.46
(D)	0	1.07	0.67	0.43	0.31

These differences are attributed to the fact that the V_{OC} is related to the difference between the Nernst potential of the redox and the Femi-level [41,48]. Since the TEM and SEM images confirmed, with further Au NPs deposition, a higher portion of the tip surface of TiO_2 nanorods is covered by Au NPs and the active part of DSSC samples and consequently overall efficiency of cells decreased. Though, due to the fact that the rate of increase in J_{SC} is greater than that of decreasing V_{OC} in the Au NPs TiO_2 nanorods DSSC, efficiency of Au NPs TiO_2 nanorods DSSC and the fill factor improved.

Fig. 9(d) shows the effect of Au NPs deposition on short circuit current at different wavelengths of light. This figure illustrates that with increasing the Au NPs the short circuit current increased and most of the current in the obtained cell is generated between 325 and 425 nm. The photocurrent increase could be partially attributed to resonant absorption due to localized plasmon modes of Au NPs, however, no distinct resonant absorption peak is observed in the spectral response. In addition, a slight reduction in the photocurrent, hence absorption, in the 500–550 nm band could be related to ohmic losses associated with resonant Au NP absorption (8–12 nm particle size) [49,50].

Table 1 indicates that the cell with 1.54 at.% Au NPs has the maximum efficiency, but with further Au NPs deposition because of a decreasing fill factor and J_{SC} overall efficiency reduced and V_{OC} shows only slight improvement. Moreover the obtained results show that overall cell efficiency for the cell with 1.54 at.% Au NPs, jumped from 0.31 to 0.94% which increased by more than twice, and the fill factor increased from 0.43 to 0.56.

4. Conclusions

Vertically aligned TiO_2 nanorod arrays were grown on FTO substrates by hydrothermal method. Different amounts of Au NPs were deposited on the TiO_2 nanorods by photoreduction method. Au NPs deposited TiO_2 nanorod dye sensitized solar cells have been fabricated and compared to cells built from TiO_2 nanorods without Au NPs. The effects of Au NPs were investigated on solar cell efficiency. Results showed that Au NPs deposited TiO_2 have presented significant improvements in fill factor and short circuit current, resulting in as much as doubled overall conversion efficiencies. Au NPs help prevent recombination by forming a Schottky energy barrier that prevents photoinjected electrons from approaching the surface of nanorod and improve the overall conversion efficiency of the DSSCs. The overall conversion efficiency was increased from 0.31% for bare TiO_2 nanorod array to 0.94% for an Au NPs deposited on TiO_2 nanorod. Moreover, measured V_{OC} results confirmed that obtained samples are quite stable and no corrosion occurs between metal NPs and the electrolyte. Most importantly, this study supports the application of Au NPs TiO_2 nanorods in improving the performance of a DSSC.

Acknowledgments

This work was supported by EU FP7 Marie Curie IRG Grant 239444, COST NanoTP, TUBITAK EEEAG Grants 108E163 and 109E044 and TUBITAK BIDEB.

References

[1] B. O'regan, M. Gratzel, Nature 353 (1991) 737.
[2] M. Gratzel, Journal of Photochemistry and Photobiology A: Chemistry 164 (2004) 3.
[3] A. Le Viet, R. Jose, M.V. Reddy, B.V.R. Chowdari, S. Ramakrishna, The Journal of Physical Chemistry C 114 (2010) 21795.
[4] S. Ueno, S. Fujihara, Electrochimica Acta 56 (2011) 2906.
[5] K. Keis, E. Magnusson, H. Lindström, S.E. Lindquist, A. Hagfeldt, Solar Energy Materials and Solar Cells 73 (2002) 51.
[6] A. Irannejad, K. Janghorban, O.K. Tan, H. Huang, C.K. Lim, P.Y. Tan, X. Fang, C.S. Chua, S. Maleksaeedi, S.M.H. Hejazi, M.M. Shahjamali, M. Ghaffari, Electrochimica Acta 58 (2011) 19–24.
[7] S. Gubbala, V. Chakrapani, V. Kumar, M.K. Sunkara, Advanced Functional Materials 18 (2008) 2411.
[8] K.A.T.A. Perera, S.G. Anuradha, G.R.A. Kumara, M.L. Paranawitharana, R.M.G. Rajapakse, H.M.N. Bandara, Electrochimica Acta 56 (2011) 4135.
[9] J. Li, H.C. Zeng, Chemistry of Materials 18 (2006) 4270.
[10] Y. Zhu, J. Shi, Z. Zhang, C. Zhang, X. Zhang, Analytical Chemistry 74 (2002) 120.
[11] P. Charoensirithavorn, Y. Ogomi, T. Sagawa, S. Hayase, S. Yoshikawa, Journal of Crystal Growth 311 (2009) 757.
[12] M. Inaba, Y. Oba, F. Niina, Y. Murota, Y. Ogino, A. Tasaka, K. Hirota, Journal of Power Sources 189 (2009) 580.
[13] M. Ghaffari, P.Y. Tan, M.E. Oruc, O.K. Tan, M.S. Tse, M. Shannon, Catalysis Today 161 (2011) 70–77.
[14] A. Michailowski, D. AlMawlawi, G. Cheng, M. Moskovits, Chemical Physics Letters 349 (2001) 1.
[15] B. Mukherjee, C. Karthik, N. Ravishankar, The Journal of Physical Chemistry C 113 (2009) 18204.
[16] D.A. Boyd, L. Greengard, M. Brongersma, M.Y. El-Naggar, D.G. Goodwin, Nano Letters 6 (2006) 2592.
[17] Y. Tian, C. Hu, X. He, C. Cao, G. Huang, K. Zhang, Sensors and Actuators B: Chemical 144 (2010) 203.
[18] C. Cao, C. Hu, X. Wang, S. Wang, Y. Tian, H. Zhang, Sensors and Actuators B: Chemical 156 (2011) 114–119.
[19] M. Paulose, K. Shankar, S. Yoriya, H.E. Prakasam, O.K. Varghese, G.K. Mor, T.A. Latempa, A. Fitzgerald, C.A. Grimes, The Journal of Physical Chemistry B 110 (2006) 16179.
[20] A. Zaban, S.T. Aruna, S. Tirosh, B.A. Gregg, Y. Mastai, The Journal of Physical Chemistry B 104 (2000) 4130.
[21] M. Adachi, Y. Murata, J. Takao, J. Jiu, M. Sakamoto, F. Wang, Journal of the American Chemical Society 126 (2004) 14943.
[22] B. Liu, E.S. Aydil, Journal of the American Chemical Society 131 (2009) 3985.
[23] M. Law, L.E. Greene, A. Radenovic, T. Kuykendall, J. Liphardt, P. Yang, The Journal of Physical Chemistry B 110 (2006) 22652.
[24] G. Li, C.P. Richter, R.L. Milot, L. Cai, C.A. Schmuttenmaer, R.H. Crabtree, G.W. Brudvig, V.S. Batista, Dalton Transactions (2009) 10078.
[25] S. Kambe, S. Nakade, Y. Wada, T. Kitamura, S. Yanagida, Journal of Material Chemistry 12 (2002) 723.
[26] N.G. Park, J. Van de Lagemaat, A. Frank, The Journal of Physical Chemistry B 104 (2000) 8989.
[27] B. Koo, J. Park, Y. Kim, S.H. Choi, Y.E. Sung, T. Hyeon, The Journal of Physical Chemistry B 110 (2006) 24318.
[28] P.T. Hsiao, Y.L. Tung, H. Teng, The Journal of Physical Chemistry C 114 (2010) 6762.
[29] T. Ohno, K. Sarukawa, K. Tokieda, M. Matsumura, Journal of Catalysis 203 (2001) 82.
[30] T. Kawahara, Y. Konishi, H. Tada, N. Tohge, J. Nishii, S. Ito, Angewandte Chemie 114 (2002) 2935.
[31] C. Karthikeyan, M. Thelakkat, M. Willert-Porada, Thin Solid Films 511 (2006) 187.
[32] E. Palomares, J.N. Clifford, S.A. Haque, T. Lutz, J.R. Durrant, Journal of the American Chemical Society 125 (2003) 475.
[33] L.E. Greene, M. Law, B.D. Yuhas, P. Yang, The Journal of Physical Chemistry C 111 (2007) 18451.
[34] M.K. Nazeeruddin, A. Kay, I. Rodicio, R. Humphry-Baker, E. Müller, P. Liska, N. Vlachopoulos, M. Grätzel, Journal of the American Chemical Society 115 (1993) 6382.
[35] S.A. Haque, Y. Tachibana, R.L. Willis, J.E. Moser, M. Grätzel, D.R. Klug, J.R. Durrant, The Journal of Physical Chemistry B 104 (2000) 538.
[36] T. Bora, H.H. Kyaw, S. Sarkar, S.K. Pal, J. Dutta, Beilstein Journal of Nanotechnology 2 (2011) 681.
[37] B.A. Gregg, F. Pichot, S. Ferrere, C.L. Fields, The Journal of Physical Chemistry B 105 (2001) 1422.
[38] V. Dhas, S. Muduli, W. Lee, S.H. Han, S. Ogale, Applied Physics Letters 93 (2008) 243108.
[39] P. Roy, D. Kim, I. Paramasivam, P. Schmuki, Electrochemistry Communications 11 (2009) 1001.
[40] C. Wen, K. Ishikawa, M. Kishima, K. Yamada, Solar Energy Materials and Solar Cells 61 (2000) 339.
[41] C.-S. Chou, R.-Y. Yang, C.-K. Yeh, Y.-J. Lin, Powder Technology 194 (2009) 95.
[42] H. Wang, Y. Bai, Q. Wu, W. Zhou, H. Zhang, J. Li, L. Guo, Physical Chemistry Chemical Physics 13 (2011) 7008.
[43] V. Zakaznova-Herzog, H. Nesbitt, G. Bancroft, J. Tse, Surface Science 600 (2006) 3175.
[44] D. Shirley, Physical Review B 5 (1972) 4709.
[45] M. Ghaffari, M. Shannon, H. Hui, O.K. Tan, A. Irannejad, Surface Science 606 (2012) 670–677.
[46] T.K. Sham, M.S. Lazarus, Chemical Physics Letters 68 (1979) 426.
[47] H. Perron, J. Vandenborre, C. Domain, R. Drot, J. Roques, E. Simoni, J.J. Ehrhardt, H. Catalette, Surface Science 601 (2007) 518.
[48] A. Zaban, S. Ferrere, B.A. Gregg, The Journal of Physical Chemistry B 102 (1998) 452.
[49] S. Link, M.A. El-Sayed, The Journal of Physical Chemistry B 103 (1999) 4212.
[50] G.W. Bryant, F.J.G. de Abajo, J. Aizpurua, Nano Letters 8 (2008) 631.